Subduction Dynamics

From Mantle Flow to Mega Disasters

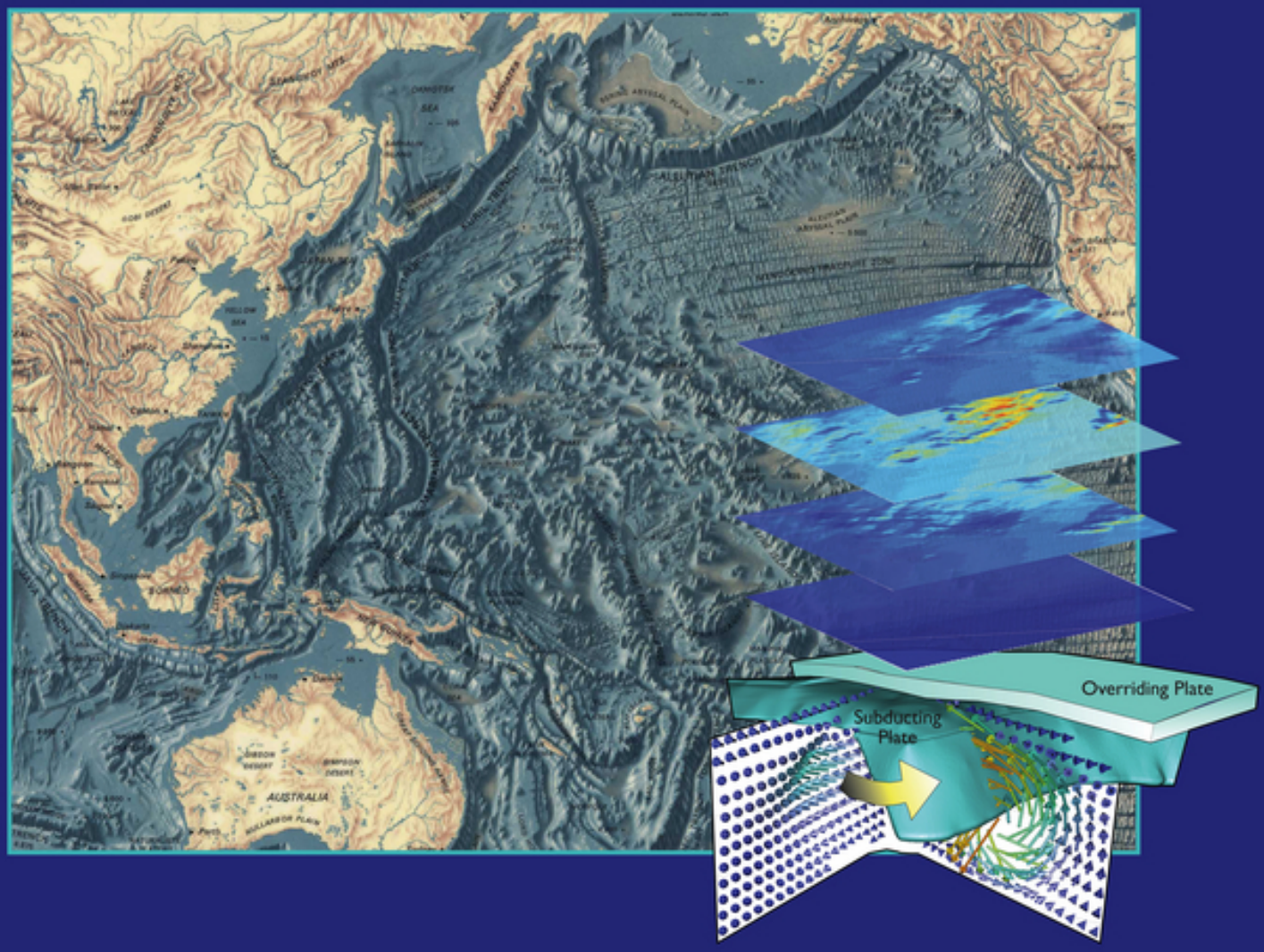

Gabriele Morra, David A. Yuen, Scott D. King,
Sang Mook Lee and Seth Stein
Editors

AGU
American Geophysical Union

WILEY

INTRODUCTION
The Impact of Subduction Dynamics on Mantle Flow, Continental Tectonics, and Seismic Hazard

Gabriele Morra[1], David A. Yuen[2], Scott D. King[3], Sang-Mook Lee[4], and Seth Stein[5]

[1] Department of Physics and School of Geosciences, University of Louisiana at Lafayette, Louisiana, USA

[2] Minnesota Supercomputing Institute and Department of Earth Sciences, University of Minnesota, Minneapolis, Minnesota, USA and School of Environmental Studies, China University of Geosciences, Wuhan, China

[3] Department of Geosciences, Virginia Tech University, Blacksburg, Virginia, USA

[4] School of Earth and Environmental Sciences, Seoul National University, Gwanak-Gu, South Korea

[5] Department of Earth and Planetary Sciences, Northwestern University, Evanston, Illinois, USA

Subduction of tectonic plates provides the main driving force for mantle convection, but also causes the greatest natural hazards such as megathrust earthquakes, often with accompanying tsunami waves. This book aims at expanding the traditional view in which subduction dynamics is usually presented, showing the wide range of natural phenomena related to the subduction process. Chapters in this book treat diverse topics ranging from the response of the ionosphere to earthquake and tsunamis, to the origin of midcontinental volcanism thousands kilometers distant from the subduction zone; from the puzzling deep earthquakes triggered in the interior of the descending slabs, to the detailed pattern of accretionary

wedges in convergent zones; from the induced mantle flow in the deep mantle, to the nature of the paradigms of earthquake occurrence, showing how they relate to the subduction process (Figure I.1).

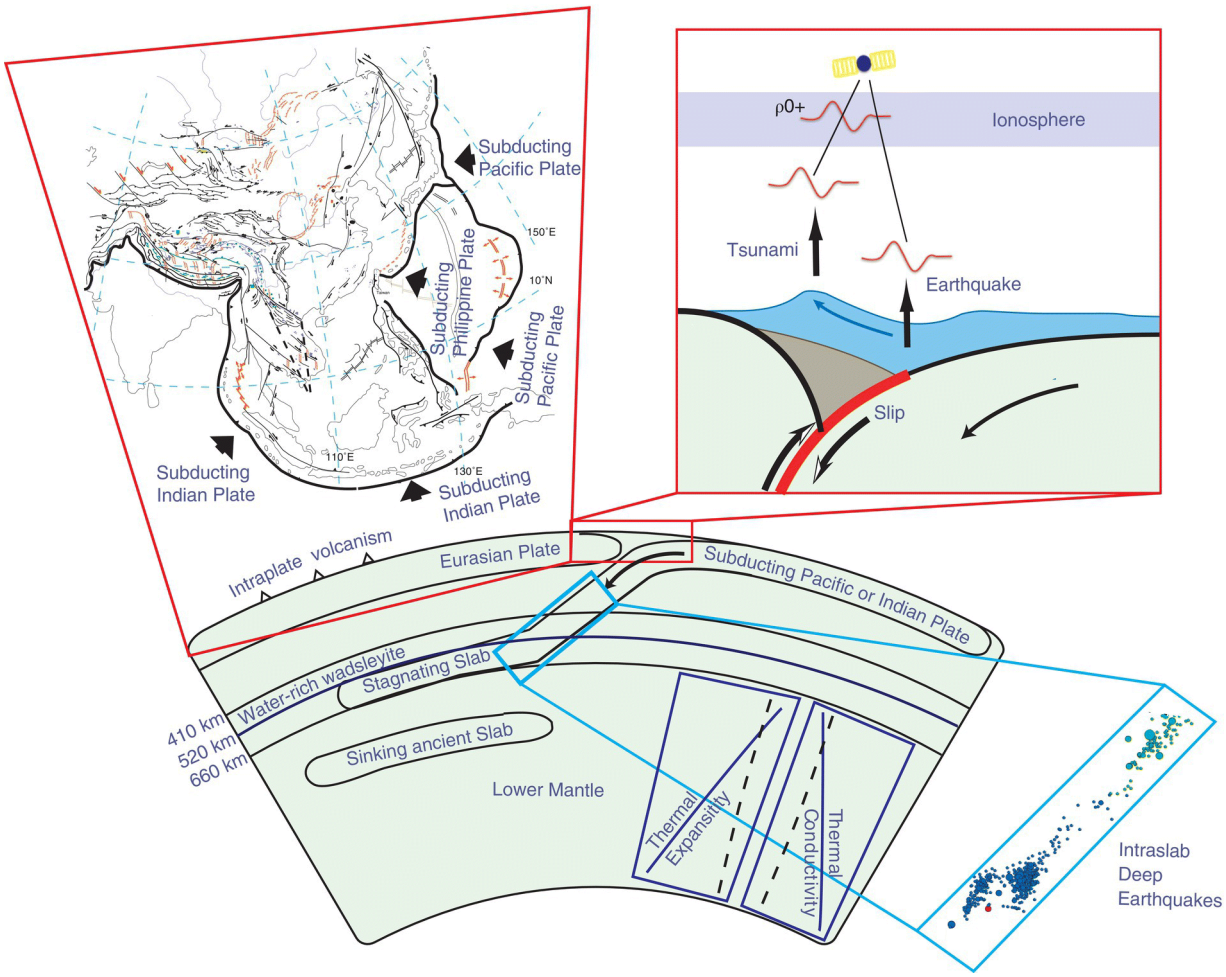
Subducting
Pacific Plate
150°E
10°N
Subducting
Philippine Plate
Subducting
Pacific Plate
110°E
130°E
Subducting
Indian Plate
Subducting
Indian Plate
ρ0+
Ionosphere
Tsunami
Earthquake
Slip
Intraplate volcanism
Eurasian Plate
Subducting Pacific or Indian Plate
Water-rich wadsleyite
Stagnating Slab
410 km
520 km
660 km
Sinking ancient Slab
Lower Mantle
Thermal
Expansivity
Thermal
Conductivity
Intraslab
Deep
Earthquakes

Figure I.1 Sketch of some of the dynamics investigated in this book. The history of the effects of the subduction process are largely observed in the tectonic structures of the overriding plate, as shown by the chapters focusing on the Eurasian continent (see Figure I.2). The most dramatic events caused by Subducting plates are the large thrust earthquakes (see Chapter 10 by *Geller et al.*). Megathrusts and tsunamis also cause waves in the ionosphere, as illustrated in the panel on the top right. Rayleigh waves propagate due to both the quake and to the tsunami (see Chapter 9 by Occhipinti). The down-going slab induces a complex mantle flow, as shown by M. A. Jadamec in Chapter 7. Inside the slab, earthquakes are detected down to the transition between upper and lower mantle, but their mechanism is still debated (see So and Yuen in Chapter 8, e.g. about the hypocenter distribution within the Tonga slab on the bottom right panel). Thermal expansivity and conductivity gradients estimates are shown in the bottom right panels. Their role in mantle dynamics is analized in *Tosi et al.*, Chapter 6.

Megathrust earthquakes are the greatest destructive earthquakes and are caused by the sudden 10–20 meter slip of hundreds of kilometers along convergent plate boundaries. Until the present, the seismic hazard relating convergent margins, where plates subduct, has been based mostly on the limited historical data derived from earthquake catalogues [*Stein et al.,* 2012]. Unfortunately, as shown by the unexpected enormous damages caused by Sumatra and Tohoku earthquakes, catalogues have proved to be too limited in scope to predict the maximum magnitude of an earthquake, or to predict the size of the attendant tsunami (see Chapter 10 by Robert Geller and colleagues). While past attempts to relate the size of the largest earthquakes to the dynamics of the slab (dip, convergence, age, presence of heterogeneities) have failed

due to their excessive simplicity, the combination of new data and improved numerical models based on thermal-mechanical principles [e.g., *van Dinther*, 2013] promises a new generation of time-dependent hazard maps that have more physics builtin.

This book is the result of a meeting that was held August 19 to 22, 2012, on Jeju Island, South Korea, with about 50 researchers from East Asia, North America, and Europe [*Morra et al.*, 2013]. On the first day of the meeting, most presentations focused on the causes of the Sumatra (2004) and Tohoku (2011) earthquakes. The opening talk was a review of the ionospheric response to subduction-induced thrust earthquakes and the associated tsunamis, which has been extended into Chapter 9 by Giovanni Occhipinti. From the presentations that followed, it emerged that the detailed analysis of the tsunami height along the coast of Tohoku is incompatible with the simple model based on the rebound of an overriding plate. Alternative possibilities were proposed from which two hypotheses emerged, one involving the release of gravitational potential energy at the accretionary wedge [*McKenzie and Jackson*, 2012], and the other the slip of a spline fault in crustal wedge, providing boost in elastic energy in driving the tsunami. While the discussion continues within the scientific community [e.g., *Tappin et al.,* 2014], this controversy shows how the seismic hazard estimation at subduction zones should be rethought to take into account the bimodal dynamics of the crustal wedge.

In order to improve our ability to estimate the seismic hazard due to the motion of the solid Earth, we must understand the details of subduction dynamics. The present paradigms emerge mainly from reconstructing and numerically modeling plate tectonics in the past. Speed of computing increased from gigaflops in 1990 to petaflops today, a factor of a million. Thus, investigation of the origin

of plate tectonics in the next 20 years is expected to rely heavily on new numerical algorithms and the ability to run numerical models on the fastest and largest supercomputers.

The pull of the slab in the upper mantle is the main driver of the motion of the plates on the surface [*King*, 2001]. The detection of plate kinematics through GPS data and their reconstruction based on the magnetic isochrones in the seafloor constrain to 10–20 Myrs the time necessary for a plate to sink through the upper mantle. At longer timescales, the dynamics behind Earth evolution are less understood [*Torsvik et al.*, 2014]. From hundreds of Myrs to Gyrs, the Wilson cycle of the formation and breakup of supercontinents, global reorganization of plate motion [*King et al.*, 2002], and cycles controlling plate size and morphology [*Morra et al.*, 2013] are only some of the global geodynamic processes that control the global Earth evolution [*Funiciello et al.*, 2008]. Five chapters of this volume focus on this long-term tectonic evolution, all of them related to the subduction process at the eastern and southern Eurasian margins. (Detailed map in Figure I.2.)

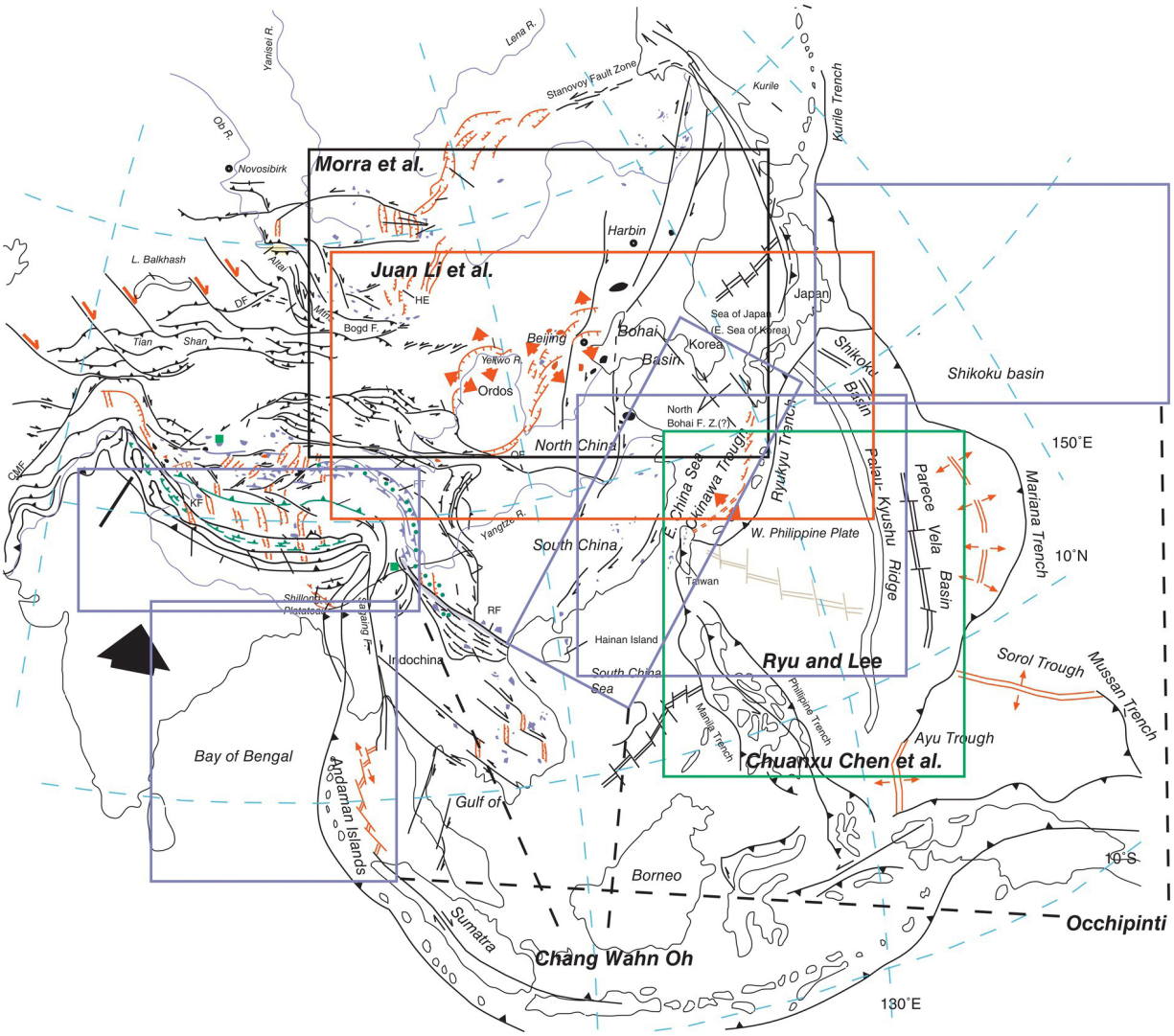

Figure I.2 Summary of the Asian regions covered in this volume overlaying a overview of the Asian tectonics. The map is modified after [*Yin*, 2010]. Chapter 2 from Chang Wahn Oh and Chapter 9 by Giovanni Occhipinti cover two separate regions.

In Chapter 4, Chuanxu Chen and coworkers analyze detailed data on accretionary wedges essential to understanding the development of thrust earthquakes. Focusing on the Manila trench, they find that the segmentation of the incoming plate correlates well with the distribution of seismicity. They suggest that the seafloor morphology might be carved by the heterogeneities created

during the rifting process and control seismicity at the precollision zone.

An investigation of the causes of the very deep earthquakes within the subducting slab is presented in Chapter 8 by Byung-Dal So and David A. Yuen. Here the authors look for a relationship between the deviatoric stress regime and the distribution of deep earthquakes in the subducted lithosphere. The authors suggest that a new mechanism based on shear heating around the 410-km phase transition and consequent reduction in elastic modulus might account for part of this seismicity.

Many talks at the Jeju meeting focused on Asian tectonics and this is reflected in this volume. In Chapter 2, Chang Whan Oh reviews the geological evidence that the Dabie-Hongseong collision belt in eastern Asia might have been caused by a westward-migration slab break-off migration from 245 Ma to 240 Ma. Using the same approach, he relates the Himalayan collision to an eastward migrating slab break-off from ~ 50 Ma to ~ 25 Ma. In Chapter 3, In-Chang Ryu and Changyeol Lee approach another mystery of Asian tectonics: the origin of the adakitic arc magmatism, which extends from South China to eastern Japan, and appeared during the Cretaceous, 140–60 Ma. They notice that the traditional hypothesis that links the volcanism to a migration of the Pacific-Izanagi ridge is incompatible with most recent plate reconstructions, and propose instead the opposite migration of an intracontinental mantle plume.

Focusing on the evolution of Asia during the Cenozoic, Chapter 5 by Gabriele Morra and coworkers investigates the causes of the volcanism in central and eastern Asia, proposing that it emerges from a volatile-rich layer at the top of the transition zone, fed by the underlying stagnating Pacific slab. They propose that the volatiles slowly rise from

the subducted crust and form fluid-rich microregions at the top of the transition zone from which they rise as clusters of diapirs.

Juan Li and coworkers, in Chapter 1, constrain the thickness of the Pacific stagnating slab beneath northeast Asia. Through the method of caustic waveform, they model both P and S waves and estimate an extra thickening of 50–60 km, supporting the hypothesis that the subducted slab may be piling up under northeast Asia, therefore partially explaining the missing slab from Pacific subduction.

Finally two chapters investigate subduction-induced mantle flow. The role of thickening of the subducted slab is addressed in Chapter 6 by Nicola Tosi and coworkers who show that the variations of thermal expansivity and conductivity with temperature and pressure induce a severe change of the strength in the downgoing slab. In particular, they find that the decrease of expansivity with depth enhances buckling and slab thickening in the lower mantle.

The response of the upper-mantle flow to subduction is addressed by M. A. Jadamec who shows in Chapter 7 how a rheological formulation closer to laboratory data, implementing a fully nonlinear mantle rheology, impacts significantly on the mantle response. She shows that the dynamical support of the mantle to the downgoing slab is reduced by the nonlinearity of the mantle-rocks creep, impacting the slab dip, the stress distribution in the slabs, and the stress state of the surface plates.

REFERENCES

Funiciello, F., C. Faccenna, A. Heuret, S. Lallemand, E. Di Giuseppe, and T. W. Becker (2008), Trench migration, net

rotation and slab-mantle coupling, *Earth Planet. Sci. Lett.*, *271*(1–4), 233–240.
King, S. D. (2001), Subduction zones: Observations and geodynamic models, *Phys. Earth Planet. Inter.*, *127*(1–4), 9–24.
King, S. D., J. P. Lowman, and C. W. Gable (2002), Episodic tectonic plate reorganizations driven by mantle convection, *Earth Planet. Sci. Lett.*, *203*, 83–91.
McKenzie, D., and J. Jackson (2012), Tsunami earthquake generation by the release of gravitational potential energy, *Earth Planet. Sci. Lett.*, *345–348*(0), 1–8.
Morra, G., M. Seton, L. Quevedo, and R. D. Müller (2013a), Organization of the tectonic plates in the last 200 Myr, *Earth Planet. Sci. Lett.*, *373*, 93–101.
Morra, G., R. J. Geller, S. T. Grilli, S. Karato, S. King, S.-M. Lee, P. Tackley, and D. Yuen (2013b), Growing understanding of subduction dynamics indicates need to rethink seismic hazards, *Eos, Transactions American Geophysical Union*, *94*(13), 125–126.
Stein, S., R. J. Geller, and M. Liu (2012), Why earthquake hazard maps often fail and what to do about it, *Tectonophysics*, *562*, 1–25.
Tappin, D. R., S. T. Grilli, J. C. Harris, R. J. Geller, T. Masterlark, J. T. Kirby, F. Shi, G. Ma, K. K. S. Thingbaijam, and P. M. Mai (2014), Did a submarine landslide contribute to the 2011 Tohoku tsunami? *Marine Geology*, *357*, 344–361.
Torsvik, T. H., R. van der Voo, P. V. Doubrovine, K. Burke, B. Steinberger, L. D. Ashwal, and A. L. Bull (2014), Deep mantle structure as a reference frame for movements in and on the Earth, *Proceedings of the National Academy of Sciences*, *111*(24), 8735–8740.
Van Dinther, Y., T. V. Gerya, L. A. Dalguer, P. M. Mai, G. Morra, and D. Giardini, (2013), The seismic cycle at subduction thrusts: Insights from seismo-thermo-

mechanical models, *J. Geophys. Res.: Sol Ea*, *118*, 6183–6202, doi:10.1002/2013JB010380.
Yin, A. (2010), Cenozoic tectonic evolution of Asia: A preliminary synthesis, *Tectonophysics*, *488*, 293–325, doi:10.1016/j.tecto.2009.06.002.

1
Evidence from Caustic Waveform Modeling for Long Slab Thickening above the 660-km Discontinuity under Northeast Asia: Dynamic Implications

Juan Li[1], Nicola Tosi[2], Petra Maierová[3], and David A. Yuen[4]

[1] *Key Laboratory of Earth and Planetary Physics, Institute of Geology and Geophysics, Chinese Academy of Sciences, Beijing, China*

[2] *Department of Astronomy and Astrophysics, Technische Universität Berlin, Berlin, Germany; Department of Planetary Physics, German Aerospace Center (DLR), Berlin, Germany*

[3] *Center for Lithospheric Research, Czech Geological Survey, Prague, Czech Republic*

[4] *School of Environment Studies, China University of Geosciences, Wuhan, China; Minnesota Supercomputing Institute and Department of Earth Sciences, University of Minnesota, Minneapolis, Minnesota, USA*

ABSTRACT

Knowledge of the thickness and age of slabs is of great importance to further our understanding of the deformation of the subducting lithosphere and, in general, of regional mantle rheology. The technique of seismic tomography has been widely used to identify thermally induced mantle heterogeneities. However, because of the contamination of complicated caustic waveforms, its resolving power is relatively poor when it comes to image slabs in the mantle transition zone. In this study, we aim at constraining the thickness of the slab in the mantle transition zone beneath northeast Asia through the method of caustic waveform modeling for both P and S waves. We detect a high-velocity layer associated with a thickened slab lying in the transition zone and estimate its thickness to be ~140±20 km, corresponding to a thickening of 50–60 km at the long-lying segment. Numerical simulations indicate that downgoing material may be piling up under northeast Asia. The part of the Pacific plate subducting at the Japan trench thus can be interpreted to be in a buckling/folding retreating mode. We argue that thickening of the slab due to buckling instabilities could partly explain the enigma of the missing Pacific slab from the Cenozoic era. In addition, the slab might be close to the threshold of instability. Based on numerical simulations, mantle circulation may become temporarily layered. Cold and dense lithospheric material, after accumulating at the 660-km discontinuity, can suddenly sink into the lower mantle, resulting in an avalanche that, perhaps, might occur in the next tens of millions of years. This will be accompanied by a resurgence of volcanic activity, precipitated by upwellings emanating from the lower mantle close to the site of the avalanche.

1.1. INTRODUCTION

Subducted oceanic slabs represent the major source of buoyancy driving mantle flow [e.g., *Ricard et al.*, 1993]. Characterizing the process of subduction is crucial to better understand the thermal and chemical evolution of our planet. In the past decades, seismic-wave tomography, based mainly on travel-time analysis, has proved able to resolve subduction-related thermal anomalies [e.g., van der Hilst, 1991; *Fukao et al.*, 2001; Huang and Zhao, 2006; *Li et al.*,

2008; Fukao and Obayashi, 2013]. However, intrinsic problems of damping-associated inversion techniques used in tomography as well as the poor resolution at depth inhibit the possibility to place robust constraints of the detailed structure of subducting slabs. A recent study devoted to quantifying the uncertainty in travel-time tomography reveals that the root mean square velocity perturbations for many acceptable models compatible with the same travel-time dataset can vary from 0.3% to 1.3% in the upper mantle [*de Wit et al.*, 2012]. Furthermore, in the transition zone, the limited ray coverage of the first arrivals caused by waveform triplication results in an even more ambiguous image.

Constraining the thickness of subducted slabs is of great importance in understanding problems related to mantle rheology and evolution of the lithosphere-mantle system. Slabs can undergo large deformation: they can bend, stretch, and thicken [*Gurnis and Hager*, 1988; *King*, 2001]. In the upper- to midlower mantle, thick blobs of seismically fast anomalies have been identified by different authors in subduction regions beneath Tonga, Marianas, and Kuril [e.g., *Creager and Jordan*, 1986; *van der Hilst*, 1995; *Fukao and Obayashi*, 2013]. Scaling laws derived from the theory of buckling of viscous sheets have been successfully employed to explain the apparent thickening of the subducted lithosphere beneath the transition zone as revealed by a few seismic studies [Ribe *et al.*, 2007]. Fully numerical simulations of viscous flow with composite rheology have been performed to further explore the possible mechanisms leading to the emergence of long-wavelength thickening of slabs in the lower mantle [*Běhounková and Čížková*, 2008]. Furthermore, 3D numerical models have shown that a relatively weak slab, with a viscosity not more than 100 times larger than that of the ambient mantle, can achieve a broad variety of shapes [Loiselet *et al.*, 2010]. In spite of this focus on slab behavior in the middle to lower mantle, different styles of slab deformation have been identified in the upper mantle transition zone. The thickness of the subducted lithosphere in the upper part of the Bullen region [*Bullen*, 1963], which was proposed to be the transition region between the upper and lower mantle, however, is not well revolved. A slab with an initial thickness of ~80–90 km [*Zhao et al.*, 1994] has been imaged beneath the Japan trench, behind which a vast amount of material lies subhorizontally over the 660-km discontinuity [e.g., *Huang and Zhao*, 2006; *Li and van*

der Hilst, 2010, *Fukao and Obayashi*, 2013] (hereafter referred to as the 660). The resolved high-velocity layer in the stagnant slab, however, seems to occupy the whole mantle transition zone with an uncertainty of around ±90 km or even more.

In this paper, we discuss our finding of a thickened slab in the upper mantle transition zone beneath northeast Asia and the possible mechanism of its formation, and we speculate on the dynamic implication associated with its fate. The constraint on the thickness of the slab is based on P and S wave models of *Li et al.* [2013] obtained from the method of caustic waveform modeling. We first show the sensitivity of the method to the structure around the 660-km discontinuity, and then briefly introduce the data sources and main features of the resolved P and S velocity models. New waveform datasets are added to verify the correctness of the obtained model, and a series of uncertainty tests based on waveform matching are performed, which provide a robust constraint on the thickness of the stagnant segment of the slab. 2D finite-volume numerical simulations were also performed in order to understand the dynamic implications of a thickened stagnant slab in the transition zone. We will argue that thickening of the slab due to buckling instability may partly explain the enigma of the missing Pacific slab. The slab may be close to be unstable, and the continuous piling up of lithospheric material may trigger an event of mantle avalanche beneath northeast Asia.

1.2. CAUSTIC WAVEFORM MODELING AND DATA SOURCES

Caustic waveforms are caused by seismic triplication [*Aki and Richards*, 2009], occurring in the presence of a first-order discontinuity with positive velocity jump or a sharp increase in velocity gradient (Figure 1.1). Because the pathways of triplicate phases lie very close to each other in the lithosphere and crust, differences in relative time and amplitude between different seismic branches, and especially the location of the caustic points (Figure 1.1b), turn out to be quite sensitive to the velocity structure around the discontinuity. For example, the location of cusp-B is sensitive to the velocity gradient in the lower-mantle transition zone right above the 660; the location of cusp-C is

sensitive to the velocity below the 660; and the travel-time difference between AB and CD branches is sensitive to velocity jump across the 660.

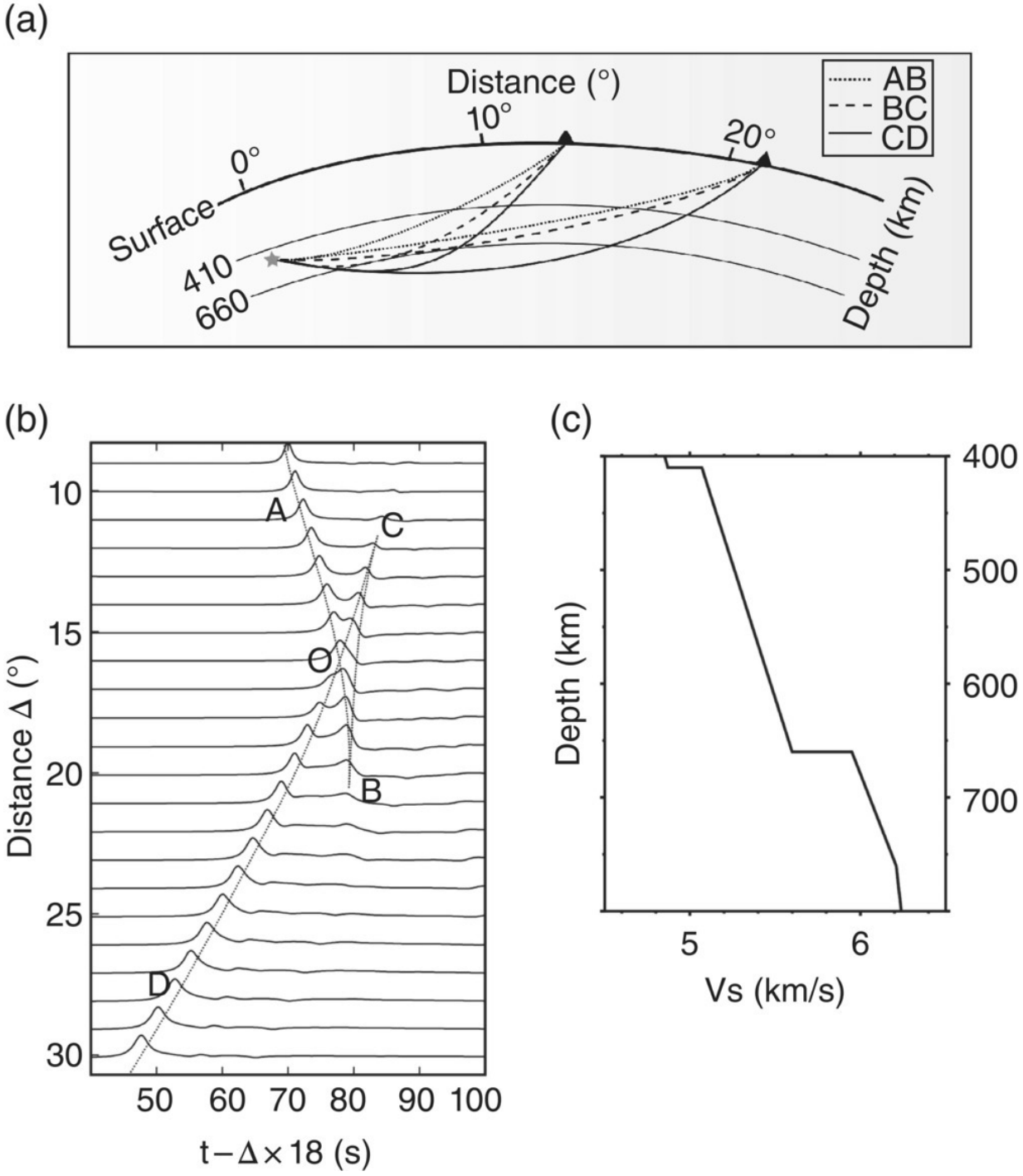
(a)
Distance (°)
10°
20°
0°
Surface
410
660
AB
BC
CD
Depth (km)
(b)
Distance Δ (°)
10
15
20
25
30
A
C
O
B
D
50
60
70
80
90
100
t − Δ × 18 (s)
(c)
Depth (km)
400
500
600
700
5
6
Vs (km/s)

Figure 1.1 Diagram of caustic waveforms. (a) Three consecutive phases are expected to arrive at the receiver side. These are the direct AB phase, a wave diving above the discontinuity; the reflected BC phase, a wave reflected from the discontinuity; and the CD phase diving below the discontinuity. (b) Synthetic transversal displacement for an assumed epicentral depth of 520 km. The locations of caustic points are very sensitive to the velocity structure around the discontinuity. (c) Iasp91 model used for the synthetic waveform calculation.

The triplication method has been applied to constrain the upper mantle discontinuities and core-mantle boundary (CMB) structure [e.g., *Lay and Helmberger*, 1983; *Grand and Helmberger*, 1984; *Wang and Yao*, 1991; *Tajima and Grand*, 1995; *Tajima and Grand*, 1998; *Brudzinski and Chen*, 2000; *Brudzinski and Chen*, 2003; *Song et al.*, 2004]. However, due to the sparse distribution of seismic instrumentations, previous studies were largely based on individual or limited seismogram analysis within a large aperture seismological array with which it is difficult to resolve the trade-off between the depth and sharpness of the discontinuity and velocity variation [e.g., *Tajima and Grand*, 1998; *Wang et al.*, 2006]. To illustrate how a velocity variation around the 660 can influence triplication waveforms, we show synthetic transversal displacements (Figure 1.2a) calculated from three different velocity models (Figure 1.2c), which are proposed to characterize deep structure in subduction regions [e.g., *Tajima and Grand*, 1998; *Wang et al., 2006*; *Wang and Niu, 2010*; *Ye et al., 2011*]. In Model 1, the 660-km discontinuity is depressed to 690 km; in Model 2, the 660-km discontinuity is a layer with a thickness of ~50 km instead of a sharp velocity jump; in Model 3, there is a gentle velocity gradient ($dV/dh = 0.0036\ s^{-1}$) across a layer with a thickness of ~60 km located just above the 660. Over a certain distance, the amplitude of AB and CD phases varies between the models. However, the differences arising from a single seismogram are not clear enough for discriminating the right model (Figure 1.2a). On the other hand, the location of cusp-B, cusp-C, and crossover point O varies significantly (Figure 1.2b). For example, the locations of cusp-B and O are shifted by 0.9° in Model 1 compared with the reference iasp91 model; the AB branch terminates at a much longer distance (~27°) in Model 3.

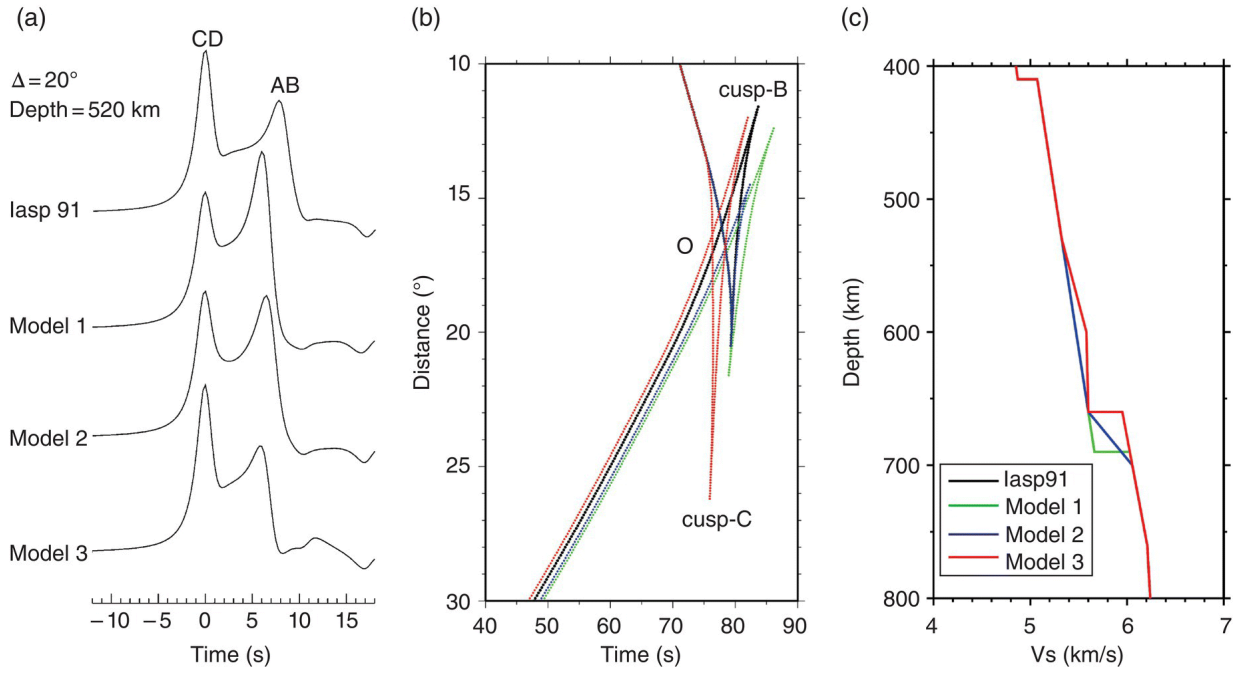

Figure 1.2 (a) Synthetic seismograms at 20° epicentral distance (Δ) for transversal component S wave calculated for iasp91 model and three different models (c). The depth of the event is 520 km. The trade-off between the depth of the interface and velocity variation around the 660-km discontinuity is not well resolved due to the similarity of the waveforms in a single seismogram. (b) Predicted caustic-wave travel-time after aligning seismograms with the epicentral distance. Significant discrepancy appeared in the major features of caustic points, which can be used to discriminate between different models. (c) Different models used for calculation of (a) and (b). Note that the reference model iasp91 (black line) is overlapped with the other three models.

With the rapidly increasing installation of broadband seismic stations, the record section of seismograms as a function of epicentral distance within a limited azimuth range becomes much more useful and reliable for exploration of the vertical deep-mantle structure [e.g., *Wang and Niu*, 2010; *Ye et al.*, 2011]. In recent years, more than 800 broadband seismic instrumentations have been installed on mainland China, making it feasible to investigate the deep-earth structure in detail through the dense array technique [*Zheng et al.*, 2010; *Niu and Li*, 2011].

The velocity structure of the mantle transition zone described in the next section is based mainly on our new findings obtained

through caustic waveform modeling [*Li et al.*, 2013]. Here we want to emphasize three important points: (1) In contrast to the traditional single or limited seismogram analysis, we take advantage of a well-constructed fan-shaped profile within a narrow azimuth range (Figure 1.3), and use the major features of the whole stack of seismic records, e.g., the location of caustic points, the crossover distance of the AB and CD branches, and the relative time between the AB and CD phases as well, with the goal of obtaining an accurate seismic image of the upper mantle transition zone beneath northeast Asia. (2) Only events with both P and SH waveforms clearly recorded (Table 1.1) are plotted in Figure 1.3. We used exactly the same station-receiver geometry for both P and SH waves to ensure a close match between the ray paths traversed by the P and S waves. (3) We considered a new dataset associated with one recent deep earthquake (20130406) that occurred near the border of China, Russia, and the Japan Sea (Table 1.1). This dataset, which is characterized by a relatively high signal-to-noise ratio (SNR) for both P and SH waves, was added to verify the overall features of aligned records and the fitness between the observation and theoretical seismograms. We also note that, compared to the dataset of the event 20080519 used in our previous study, the waveform of this new event seems to be a little noisy, and only 35 stations are selected. Therefore, we did not update the velocity models by using all those events simultaneously. The modification to the model is small considering the uncertainty estimates that will be addressed in the following section.

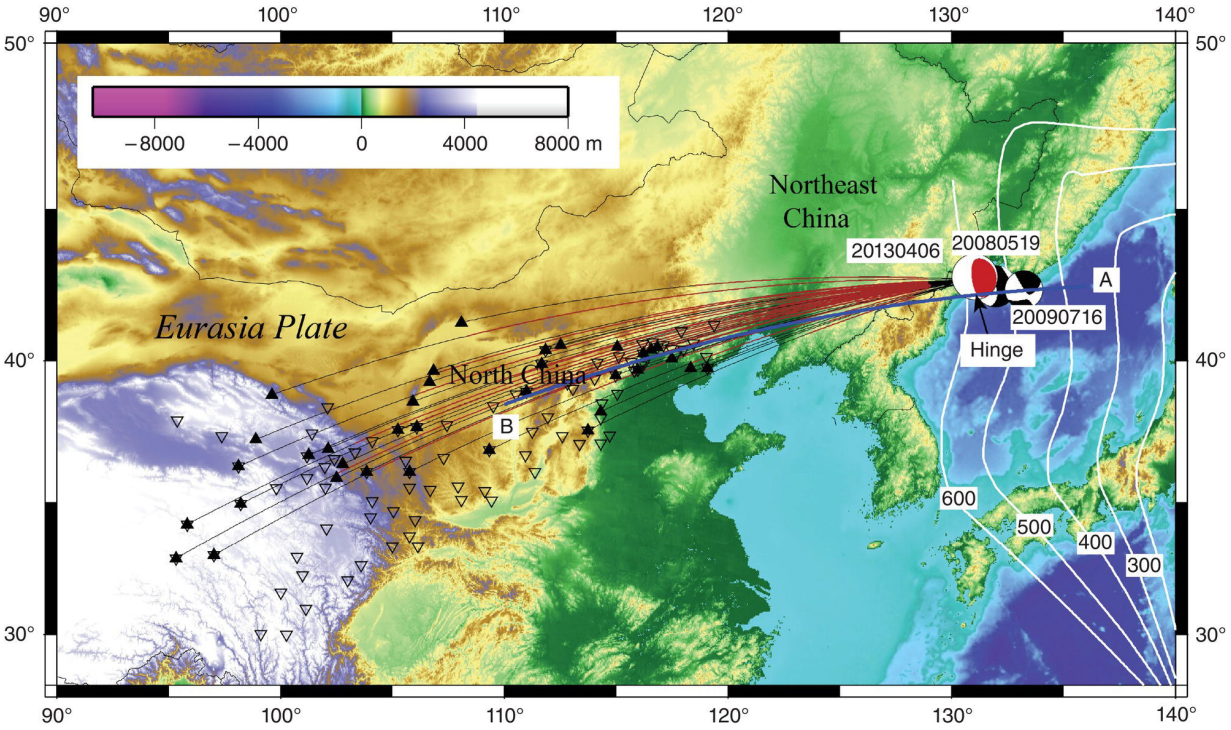

Figure 1.3 Map showing the location of deep earthquakes and regional seismic stations. The beach-ball symbols mark deep earthquake events used for caustic waveform modeling in our paper and previous study [*Li et al.*, 2013], with the red ball indicating the new event. Only events with both P and SH waveforms clearly identified are shown here. The filled triangles represent Chinese regional seismic network stations used for the new event, and the inverted blank triangles represent stations used in our previous study. Brown lines bounded by two sections of black lines highlight portions of the ray traveling below the 660 for event 20130406. The thick blue line AB marks the cross section in Figure 1.8, with “Hinge” indicating the location where the subducting slab encounters the 660 [*Li et al.*, 2008].

Table 1.1 Information of earthquakes used in caustic waveform modeling.

Event ID	Origin time	Location		Magnitude	Depth (km)		
		Lat. (°)	Lon. (°)	Mw	PDE	CMT	Used
20080519[a]	19/05/2008 00:08:36.31	42.50	131.87	5.6	513	522	519
20090716[a]	16/07/2009 06:29:04.76	42.37	133.00	5.3	477	485	477
20130406	06/04/2013 00:29:55.00	42.73	130.97	5.8	563	575	570[b]

[a] Events are from *Li et al.* [2013]. Only events with both P and SH waveform used are illustrated here and in Figure 1.3.

[b] Depth determined by array stacking method [*Li et al.*, 2008].

1.3. SLAB IMAGE IN THE MANTLE TRANSITION ZONE

The comparison between the observed and synthetic seismograms calculated from our preferred models for the new event is shown in Figure 1.4. A reflectivity synthetic code [*Wang*, 1999] is applied to generate theoretical seismograms, and a Gaussian wavelet is used to represent the source-time function. The preferred P and SH velocity models obtained from caustic waveform modeling are shown in Figure 1.5.

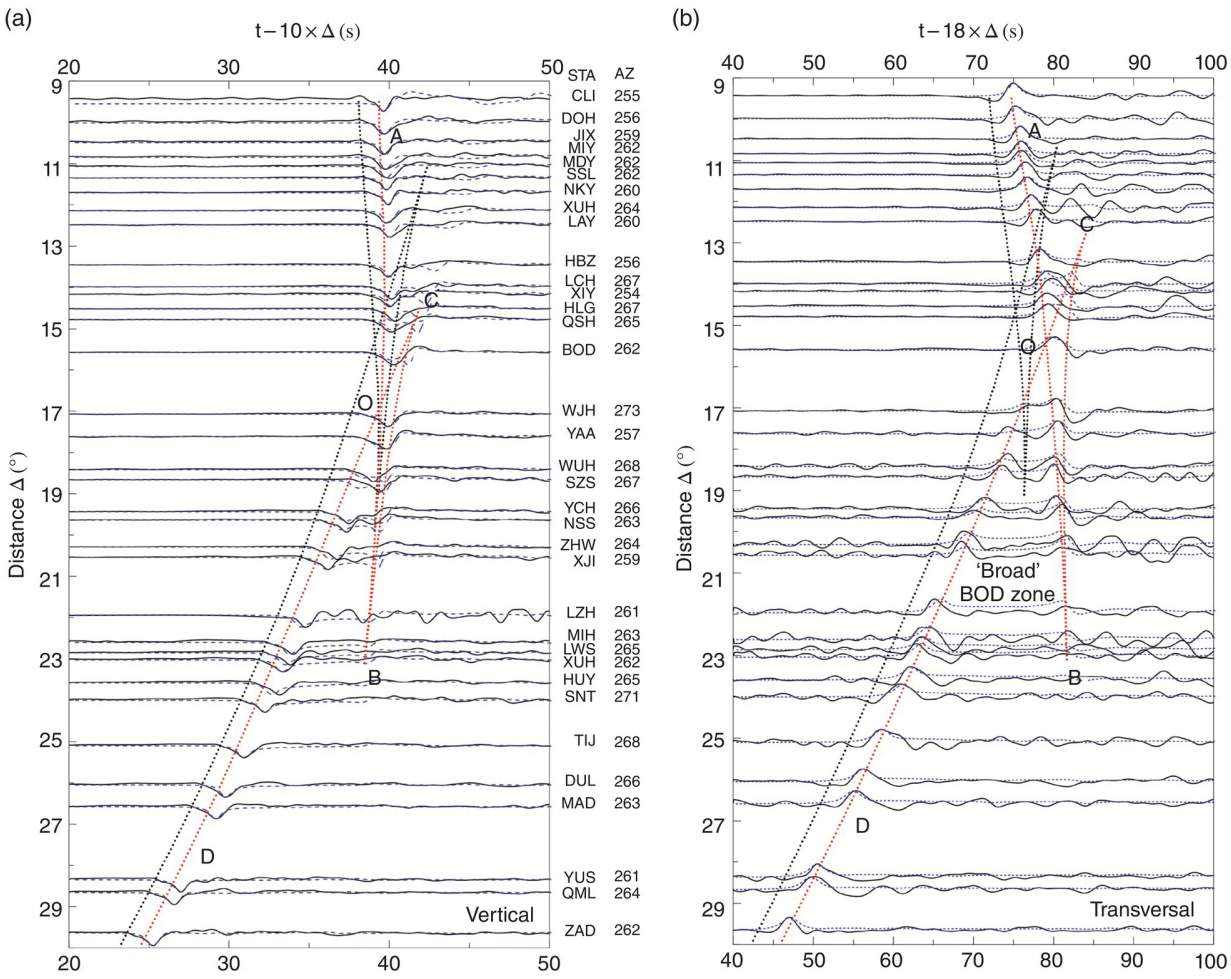

Figure 1.4 Comparison of the observed (black solid line) and synthetic waveforms (blue dashed line) calculated from the preferred P and S velocity models for the new event 20130406. (a) and (b) refer to vertical and transversal waveforms, respectively.

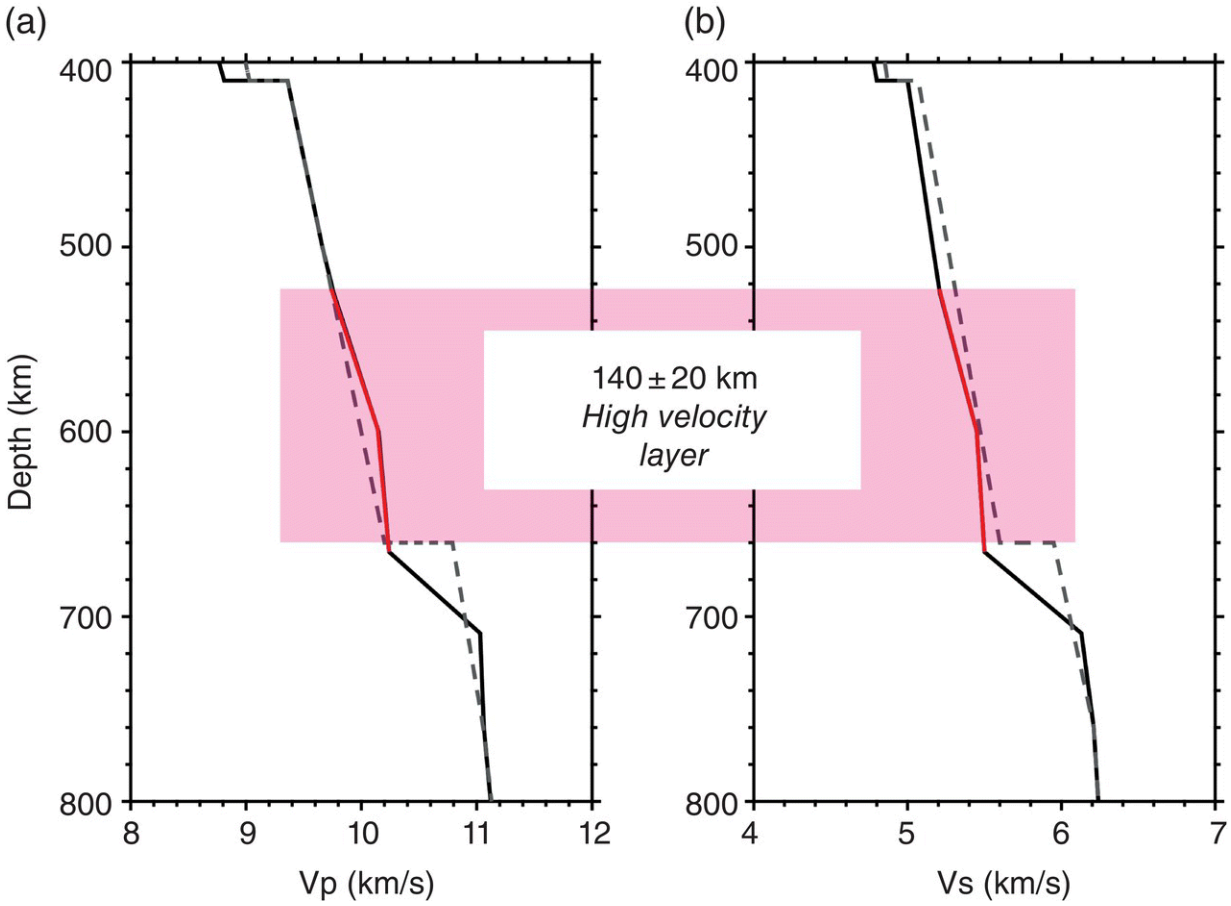

Figure 1.5 Velocity models obtained from caustic waveform modeling: (a) V_P model; (b) V_S model [*Li et al.*, 2013].

For the transversal component, the observed AB branch extends to as far as 23°, much farther than ~19° as predicted by iasp91 reference model; the CD branch begins to emerge at a distance of ~12.5°, in contrast to ~10.5° predicted by iasp91. We clearly observe a broadened BOD-zone with significantly delayed AB wave after a distance of 16°, consistent with our previous study. In the aligned vertical waveforms, the AB phase appears to be weaker around a distance of 23°; the CD phase begins to emerge around 13°, much farther than the value of ~11° calculated from the iasp91 model. Due to the limitations imposed by the station coverage, it is difficult to determine exactly the crossover distance of AB and CD phases for both types of waveform. For the detailed description of the caustic waveform modeling and comparison of seismic waveforms of other previous events, we refer the reader to *Li et al.* [2013].

In Figure 1.4, we can see that locations of caustic points and crossover distance of different branches as well as the relative time difference are matched well overall for both vertical and transversal components. Although there is some mismatch between the synthetic and observed waveforms, we argue that the local shallow structure and lateral velocity variations may contribute to this discrepancy. Waveform modeling for a 3D velocity structure should be applied to account for lateral velocity variations and for the interaction between the slab and deep mantle.

One of the major features of both P and SH models is that a high-velocity layer with a thickness of ~140 km lies just above the 660-km discontinuity (Figure 1.5), which could not be well constrained from seismic tomographic images [e.g., *Huang and Zhao*, 2006]. The slab appears to be significantly thickened in the upper mantle transition zone when compared with its initial thickness of ~80–90 km [*Zhao et al.*, 1994] near the Japan trench. To our knowledge, this is the first time the thickness of the stagnant slab in the mantle transition zone is self-consistently resolved from both P and S waveforms. Thickened and broad fast velocity anomalies in the lower mantle beneath subduction zones have been recognized by several authors [e.g., *Ribe et al.*, 2007; *Ren et al.*, 2007; *Běhounková and Čížková*, 2008]. However, seismic investigation of the thickening of slabs at the bottom of the upper mantle as well as the dynamic implications of this process are quite limited. In the following sections, we will mainly pay attention to this point. We will first present an analysis of the uncertainty for our estimate of the slab thickness; we will then discuss results from numerical simulations in order to explore possible mechanisms and implications of slab thickening in the mantle transition zone.

1.4. UNCERTAINTY ESTIMATES OF THICKNESS OF SLAB

Because of the great trade-off between depth of discontinuity and velocity variation, it is hard to provide a quantitative and accurate uncertainty estimate of the obtained velocity model. We adopted here a scheme similar to *Brudzinski and Chen* [2000]. We explored the model by perturbing the best fitting models until synthetic seismograms showed large misfits in the locations of cusp-B, cusp-

C, and O point, or in relative time between AB and CD phases. We focused on two parameters: the thickness of the higher-velocity layer just above the 660 and the velocity variation above the 660. While perturbing one parameter, we tried to keep the other parts of the structure undisturbed. We rejected perturbations that produced misfits larger than ±0.5 s in relative time between AB and CD phases, or 0.5° shift in either cusp-B, cusp-C, or O location relative to the preferred models. We choose these values because significant discrepancies of the major features will appear in the aligned waveforms. However, different cut-off of these values will definitely affect the uncertainty estimation of the slab thickness to some degree.

A series of uncertainty tests was made based on waveform matching. Figure 1.6 shows how the locations of caustic points (cusp-C and cusp-B), crossover distance (point O), and relative time between the AB and CD branches change upon perturbing the thickness of the 660. If we take the above-mentioned rules to be the standard for acceptable models, we arrive at an estimated thickness of the slab to be 140 ± 20 km, which yields a much better constraint to the thickness of the stagnant slab trapped in the mantle transition zone (Figure 1.5).

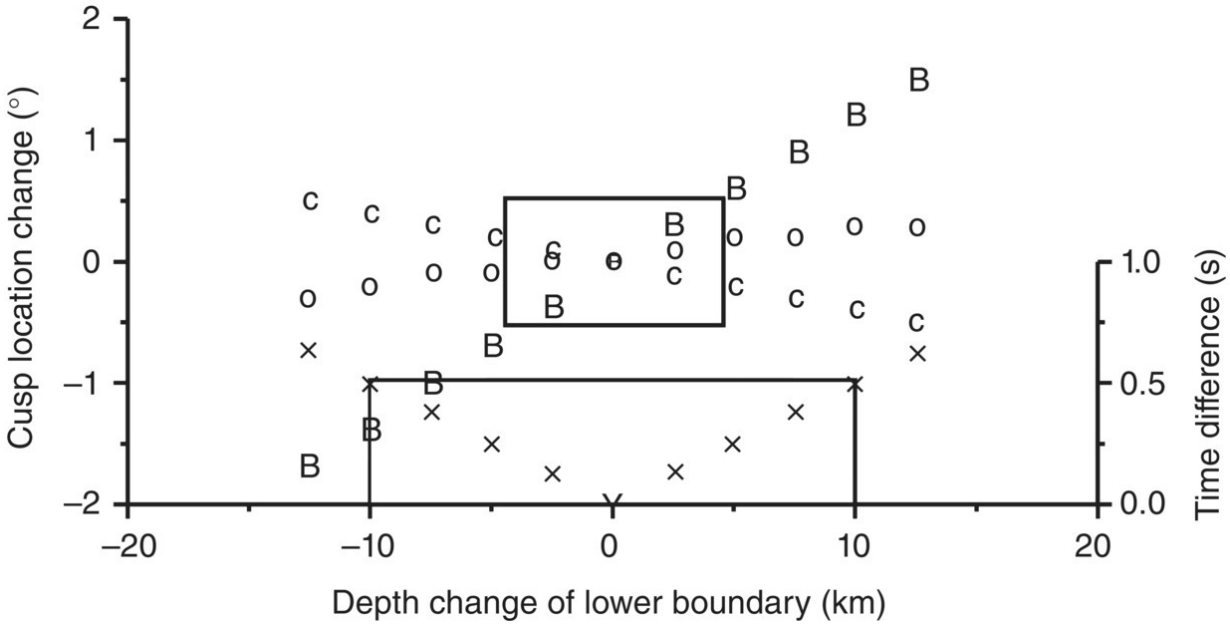

Figure 1.6 Uncertainty estimation of the slab thickness. We explore the model by perturbing the best fitting models until synthetic seismograms show large misfits in the location of cusp-B (B marks), cusp-C (C marks), and O point (O marks) or in the relative time between AB and CD phases (X marks). If the variation of the upper boundary is taken into account, the uncertainty in the thickness of the slab is estimated to be ±20 km.

1.5. DYNAMIC SIMULATION OF SLAB THICKENING

We carried out a series of 2D Cartesian numerical simulations of subduction that can help obtain a better physical understanding of the mechanisms and implications of a thickened slab. The finite-volume-based code YACC was used for the simulation [e.g., *Tosi et al.*, 2013]. YACC has been benchmarked for non-Boussinesq thermal convection [*King et al.*, 2010]. In Figure 1.7, we show three snapshots of the temperature field obtained from a simulation in which a significant thickening of the slab upon interaction with the 660-km discontinuity is observed. These results are from the reference model described by *Tosi et al.* in Chapter 6 of this volume, to which we refer for a detailed description.

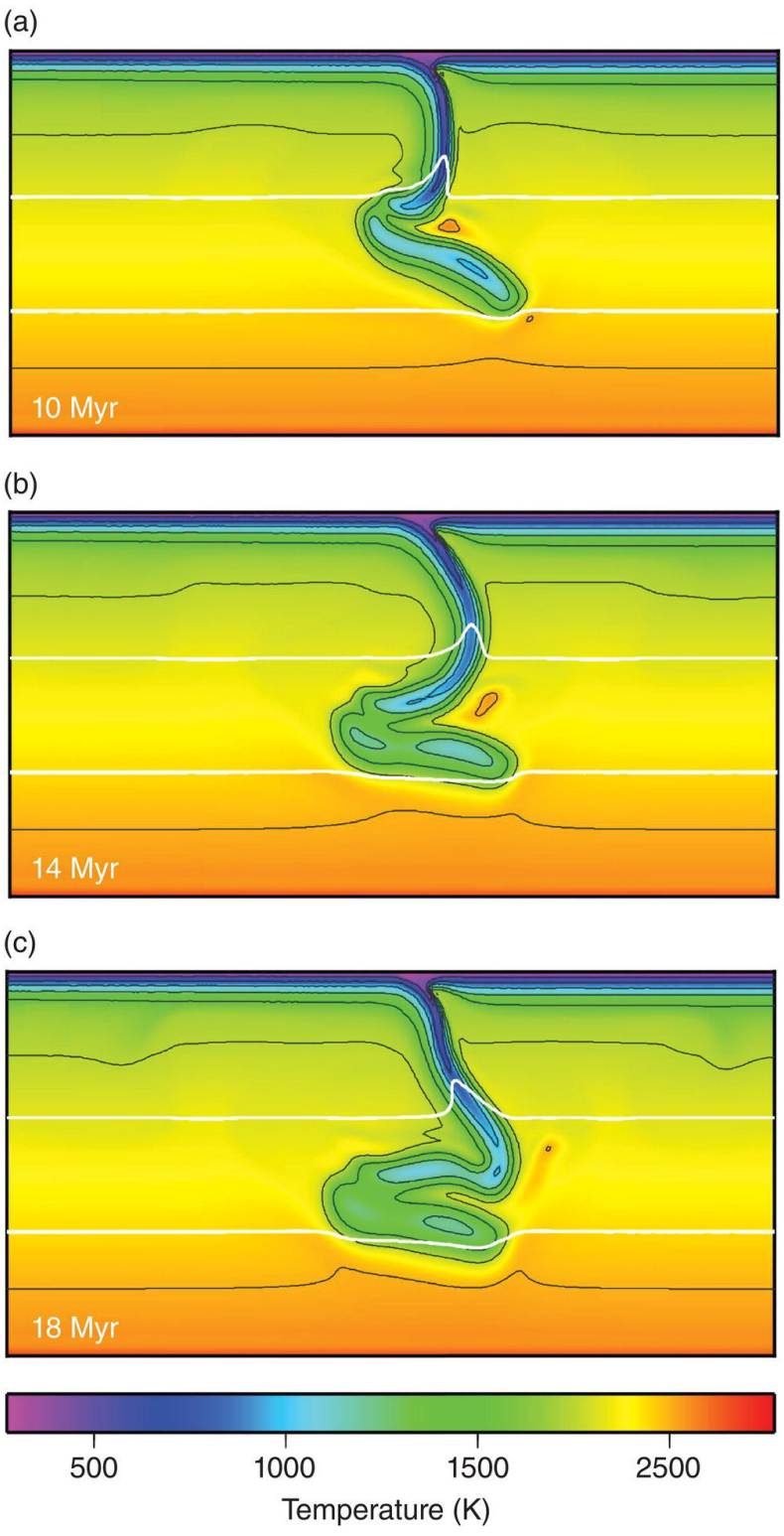
(a)
10 Myr
(b)
14 Myr
(c)
18 Myr
500
1000
1500
2500
Temperature (K)

Figure 1.7 Numerical simulation from a model of purely thermal subduction. We applied a mixed rheology: brittle with surface yield stress of 500 MPa, along with Newtonian and power-law with n = 3.5 (with different activation parameters for the upper and lower mantle). (a) The slab goes down until encountering the 660-km discontinuity; (b) Buckling instabilities occur; (c) Upon buckling, the slab material keeps piling up above the 660-km discontinuity, and the thickness of the slab is enhanced eventually. Details of model setting can be found in Chapter 6 by *Tosi et al*.

Here we list the essential features of the model. In the framework of the Extended Boussinesq Approximation [e.g., *Christensen and Yuen*, 1985] with variable thermal expansivity and conductivity [*Tosi et al.*, 2013], we employed a purely thermal convection model in a two-dimensional box with a depth of 2890 km and width of 11,560 km. A 20-km wide weak zone inclined by 30°, with a viscosity of 10^{20} Pa·s is prescribed between an oceanic and an overriding plate. At the trench, the oceanic plate has a thickness of 100 km and a temperature distribution corresponding to that obtained from a half-space cooling model for an age of ~120 Ma. The overriding plate, which is assumed to have a uniform thickness of 100 km and an age of 120 Myr, is kept fixed with a no-slip upper-boundary condition throughout the simulation. After initiating the subduction kinematically by prescribing for the subducting plate a surface velocity of 5 cm/a over a time interval of 4 Myr, we changed its boundary condition to free slip, thereby allowing the slab to fall under its own weight. We took into account the effects on buoyancy and latent heat due to the exothermic phase transition from olivine to spinel at 410-km depth, and to the endothermic one from spinel to perovksite at 660-km depth. In addition, we imposed a 10-fold viscosity jump at the 660-km discontinuity and considered pressure-, temperature-, and phase-dependent coefficients of thermal expansion and conduction following the parameterization introduced by *Tosi et al*. [2013].

Returning now to Figure 1.7, the slab descends along the weak zone and quickly starts to sink nearly vertically because of the choice of keeping the trench at a fixed position. The negative thermal buoyancy drives the slab until it encounters a significant resistance near the 660-km discontinuity (Figure 1.7a), which is caused both by the endothermic ringwoodite-perovskite phase